Petroleum Science 19 (2022) 1735–1744

Contents lists available at ScienceDirect

Petroleum Science

journal homepage: www.keaipublishing.com/en/journals/petroleum-science

Original Paper

Shaly detritus embedded epoxy-resin coated proppants

Zhao-Hui Lu [a, 1], Xiu-Ping Lan [b, 1], Yong Yuan [a], Jian-Kun Zhou [a], Si-Yuan Chen [b], Fan Fan [b], Ying-Chun Niu [b], Shou-Zhen Li [b], Kai-Yi Hu [b], Yang Zhou [b, *], Quan Xu [b, **]

[a] Key Laboratory of Shale Gas Exploration, Ministry of Natural Resources, Chongqing Institute of Geology and Mineral Resources, Chongqing, 401120, China
[b] State Key Laboratory of Petroleum Resources and Prospecting, Beijing Key Laboratory of Biogas Upgrading Utilization, Harvard SEAS-CUPB Joint Laboratory on Petroleum Science, China University of Petroleum (Beijing), Beijing, 102249, China

ARTICLE INFO

Article history:
Received 2 November 2021
Received in revised form
24 March 2022
Accepted 27 March 2022
Available online 30 March 2022

Edited by Yan-Hua Sun

Keywords:
Coated proppant
Shaly detritus
Hydrophobicity
Conductivity

ABSTRACT

Proppant plays a significant role in the hydraulic fracturing process, which can affect the production of oil and gas wells. Due to the high density and low adhesion force, the settling speed of traditional proppants is fast, which will lead to the blockage of a crack channel. In this study, a proppant with double layer structure is fabricated by coating epoxy-resin and shaly detritus on ceramic proppants for the first time, respectively. The epoxy-resin enables the shaly detritus to be coated on the proppant successfully, which can provide a new method for shaly detritus treatment. The adhesive ability of shaly detritus and epoxy-resin coated proppants (SEPs) is improved by 10.4% under the load force of 500 nN, which prolongs the time for the fracture to close. At the same time, the suspending ability of SEPs is two times higher than the uncoated proppants. Once the guar gum solution concentration is 0.3 wt%, the settling time of SEPs is 36.7% longer than that of the uncoated proppants, which can effectively reduce the settlement of proppants in the crack. In addition, the hydrophobicity of the SEPs is enhanced, which reduces the water-oil ratio of crude oil and increases the liquid conductivity tested by deionized water. In summary, this new proppant is expected to promote the development of unconventional oil and gas resources.

1. Introduction

Shale oil is of unconventional oil and gas resource (Kim, 2020; He et al., 2021). The successful development of shale oil can provide energy continuously, which will reduce the dependence on external energy of China (Xu et al., 2019; Wang et al., 2019; Li et al., 2020). Hydraulic fracturing is considered to be an effective method to improve unconventional oil and gas recovery (Cheng et al., 2020; Zhang, 2014; Hu et al., 2018). It continuously injects viscous fluids into the ground until fluid pressure is sufficient to fracture formation. (Thomas et al., 2019). Proppant is a critical material in hydraulic fracturing, which could withstand high closure stresses to support the fractures from closing (Tang et al., 2018; Wang et al., 2018a; Bandara et al., 2020). The proppants are pumped into the fracture with the fracturing fluid to keep fractures open (Li et al. 2018a, 2018b; Osiptsov. 2017). With the development of hydraulic fracturing technology, various materials have been used as proppants such as rounded silica sand, glass balls, and aluminum balls, etc. Due to density, cost, and particle size reasons, glass ball- and aluminum ball-based proppants are rarely used (Reinicke et al., 2010; Mocciaro et al., 2018; Liu et al., 2015). Nowadays, ceramic proppants and resin-coated proppants are currently the most widely used proppants in hydraulic fracturing (Xie et al., 2019; Wu et al., 2017; Zhang et al., 2017a; Yao et al., 2019).

Ceramic proppants are artificial proppant, which are mainly made by bauxite and kaolin (Feng et al., 2021; Neto et al., 2015). Ceramic proppants have a higher anti-fragmentation rate and better thermal/chemical stability (Li et al., 2018c; Cui et al., 2017; Man and Wong, 2017). However, ceramic proppants have the disadvantages of high density, complex manufacturing process, and high cost, which limits their widespread usage (Wang et al., 2018b; Hao et al., 2018; Ren et al., 2019). Compared with the ceramic proppants, the density of resin-coated proppants is lower, which is easier to be spread to the upper and distal fracture (Wei et al., 2020; Zhang et al., 2017b). At the same time, the resin-coated proppants have larger strength due to the higher sphericity, which can provide high stack density to improve the pack strength. During the

* Corresponding author.
** Corresponding author.
E-mail addresses: zhouyang@cup.edu.cn (Y. Zhou), xuquan@cup.edu.cn (Q. Xu).
[1] Zhao-Hui Lu and Xiu-Ping Lan contributed equally to this work.

https://doi.org/10.1016/j.petsci.2022.03.022

hydraulic fracturing process, a small amount of resin-coated proppants will be mixed with normal proppants, which will increase the efficiency of oil and gas exploitation and reduce the usage of normal proppants to reduce the cost of proppant (Xu et al., 2021; Lan et al., 2020; Zhang et al., 2015).

In this work, for the first time, we have fabricated shaly detritus coated proppants successfully. Shaly detritus is a kind of drilling waste, traditional drilling waste treatment methods, such as calcination and landfill, will pollute land and air. This preparation method of SEPs makes the shaly detritus was flowed back to the ground with proppants without polluting the environment. SEPs have a two-layer structure, the resin layer acts a shell coated on the ceramic proppant core, and the shaly detritus layer is adhered on the surface of the resin layer. The adhesion force of the coated proppant increased by 10.4% when the load force is 500 nN, which makes the SEPs easier to adhere to the surface of the fractures. The suspending ability of SEPs is twice that of the uncoated proppants, which will improve the liquid conductivity. At the same time, the settling time of the SEPs is longer 36.7% than that of the uncoated proppants under the guar gum solution concentration is 0.3%, which will make the SEPs migrate farther in the shale fractures. Besides, the contact angle of the SEPs increased by 13.0% and 13.4% in water and the guar gum solution, respectively, which will improve the permeability of the oil phase and ultimately improve the liquid conductivity.

2. Materials and methods

2.1. Materials

The experimental materials mainly include ceramic proppants (40/60 mesh), guar gum, epoxy-resin e51, curing agent T31, and absolute ethanol.

2.2. Preparation of SEPs

Fig. 1 shows the preparation process of SEPs (see Video: preparation process of SEPs.mp4). The ceramic proppants were added to the epoxy-resin liquid prepared in a fixed mass proportion (epoxy-resin e51: curing agent = 3:1) and stirred at 300 rpm for 3 min. Then the shaly detritus was added to the mixed liquid in a fixed mass proportion (shaly detritus: epoxy-resin e51 = 3:7). The mixed

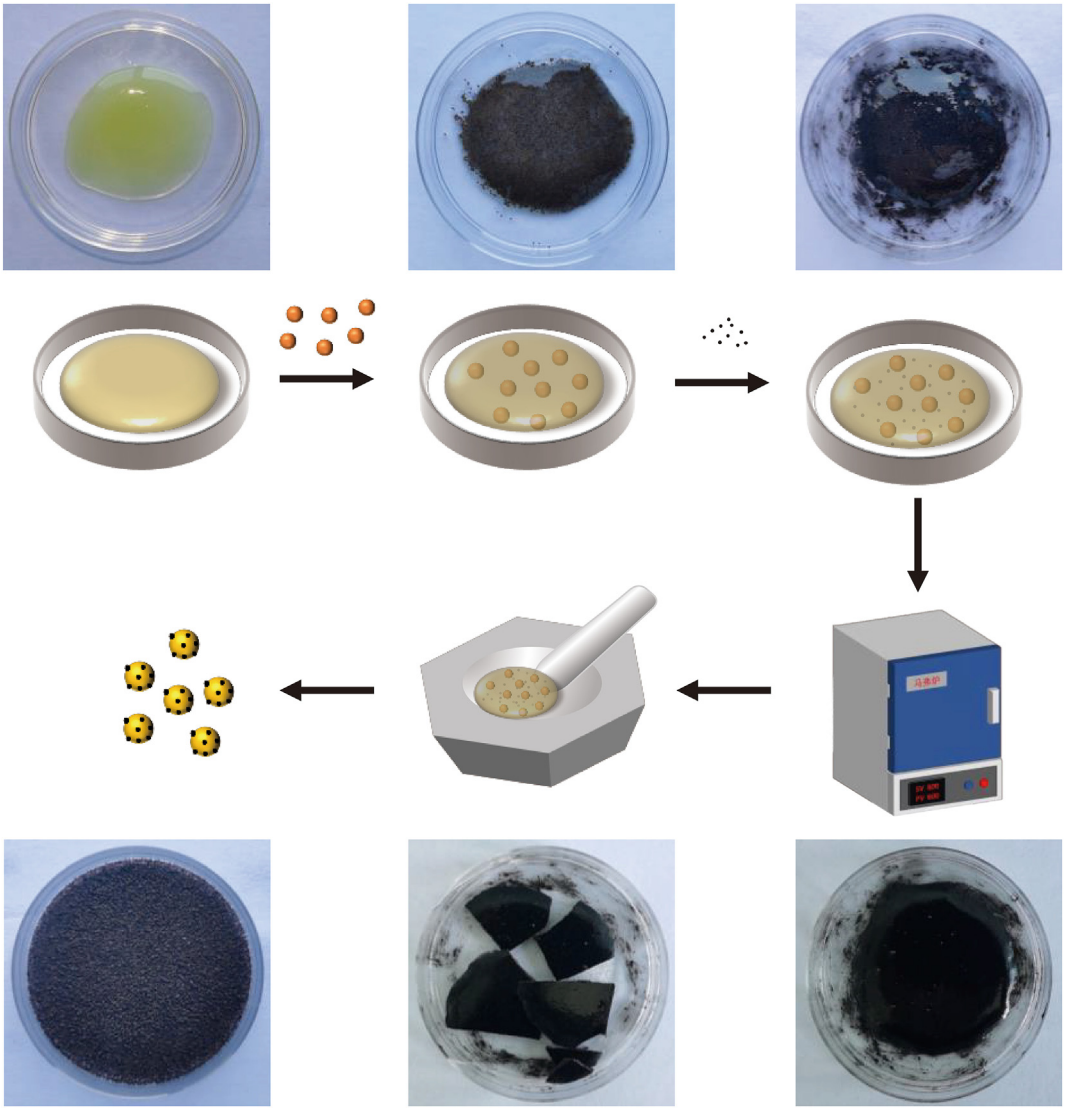

Fig. 1. Schematic diagram of preparation process of SEPs.

liquid was heated in an oven at 60 °C for 10 min. After heating, the mixed liquid was taken out and dried at room temperature for 1 h. Finally, the cooled block-shaped proppant was ground and screened.

2.3. Adhesive experiment

The adhesion force of proppant was measured by an atomic force microscope (AFM). The SEPs was placed on the sample stage. The AFM probe was manipulated to contact the surface of the proppant, which can test the adhesion force of the proppant at different conditions.

2.4. Suspending experiment

A total of 5 g SEPs was added to the guar gum solution. The solution was stirred at a stirring rate of 400 r/min for 10 min. The SEPs floated on the surface of the solution were collected and dried after stirring. The suspending ability (proppant weight on the surface/proppant weight at the bottom) of SEPs was calculated. And the suspending ability of ceramic proppant was calculated under the same condition.

2.5. Characterization

SEM and EDX images of the samples were captured using a scanning electron microscope (SEM, Zeiss sigma 500) and an energy dispersive X-ray spectrometer (EDS, Bruker Xflash 6/30). Optical contact angle measuring instrument (SDC-200) was used to measure the contact angle between proppant and water and guar gum solution (0.2 wt%). The test accuracy of the optical contact angle measuring instrument (SDC-200) is 0.1°. The test temperature and pressure of the contact angle are 25 °C and 101.325 kPa, respectively. The liquid conductivity of the proppant was measured by the liquid conductivity tester FCS-842.

3. Results and discussion

The structure of shaly detritus and epoxy-resin coated proppants has been shown in Fig. 2a. Epoxy-resin was coated on the surface of commercial ceramic proppants, then shaly detritus was coated on the epoxy-resin surface. The scanning electron microscope (SEM) images and diagram of the surface morphology of the ceramic proppant, epoxy-resin, and shaly detritus are shown in Figs. S1–S2 (see electronic supplementary material). As shown in Fig. 2b, the scanning electron microscope (SEM) image of the surface morphology indicates that the surface of ceramic proppants is uneven. Fig. 2c and d displays the SEM images of epoxy-resin coated proppant and SEP. It can be seen from the results that the shaly detritus successfully adhered to the proppant.

Fig. 3a-r shows the energy-dispersive X-ray spectroscopy (EDX) results of ceramic proppant, epoxy-resin coated proppant, and SEP. It is found that the surface of ceramic proppant is silicon element (Fig. 3b) and aluminum element (Fig. 3c). Once the epoxy resin is

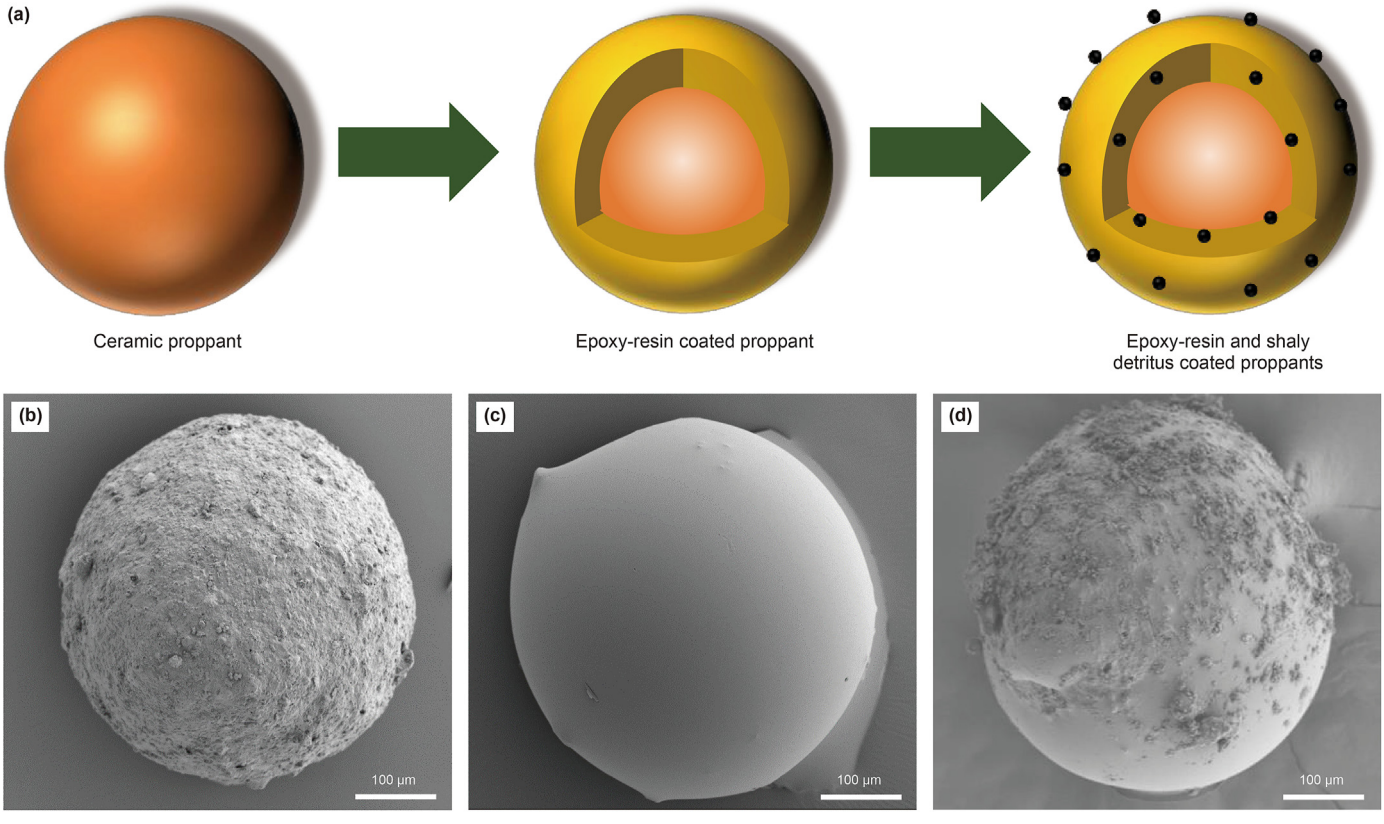

Fig. 2. (**a**) Diagrammatic sketch of the coating. SEM images of ceramic proppant (**b**), epoxy resin-coated proppant (**c**) and SEP (**d**), respectively.

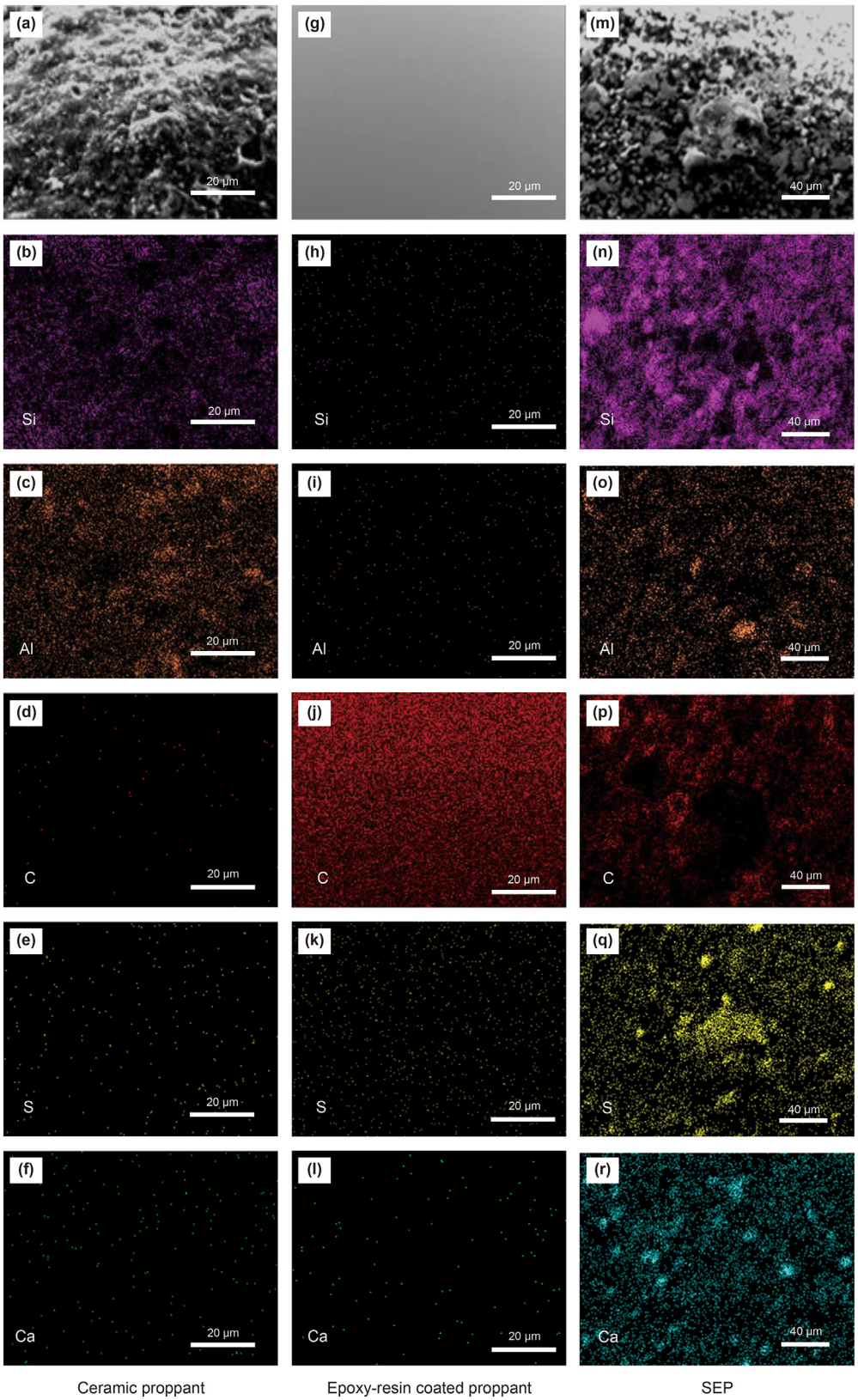

Fig. 3. SEM images of ceramic proppant (**a**), epoxy-resin coated proppant (**g**) and SEP (**m**). Distributions of silicon (**b, h, n**), aluminum (**c, i, o**), carbon (**d, j, p**), sulfur (**e, k, q**), and calcium (**f, l, r**) on the surface of ceramic proppant, epoxy-resin coated proppant and SEP, respectively.

coated to the surface of the proppant, carbon element can be found on the surface (Fig. 3j), the silicon element (Fig. 3h) and aluminum element (Fig. 3i) are almost disappeared, while the sulfur element (Fig. 3k) and calcium element (Fig. 3l) remained almost unchanged. Once the shaly detritus is coated, the silicon (Fig. 3n), aluminum (Fig. 3o), sulfur (Fig. 3q), and calcium element (Fig. 3r) are on the surface of the SEP increase, while the carbon element (Fig. 3p) decrease. This result proves that shaly detritus is successfully coated to the surface of the proppant.

3.1. Adhesive ability

Fig. 4a shows the diagrammatic sketch of the adhesion force test. Adhesion force is the ability of a material to adhere to the surface of another material. As shown in Fig. 4b, the typical AFM force curve illustrates that the adhesion force is determined by the difference between extended and retracted force curves. The adhesion force of SEPs is larger than that of uncoated proppants, which will make the proppants easier to adhere to fractures and enhance the ability of liquid conductivity.

Fig. 5a shows the variations of adhesion forces between SEPs and uncoated proppants in different load force conditions. The adhesion force of SEPs and uncoated proppants keep the same growth trend when the load force increased from 500 to 2000 nN, which illustrates that the shaly detritus did not change the relationship between the adhesion force and the load force. As the adhesion force of the SEPs is larger than that of the uncoated proppants under the same conditions, which is 10.4%, 1.9%, 4.8%, 4.1% higher, respectively. Fig. 5b displays the relationship between contact time and adhesion force. Once the contact time increased from 0.5 to 3.0 s, the adhesion force of SEPs was kept at 124 nN. The statistics show that there was no obvious change in adhesion force

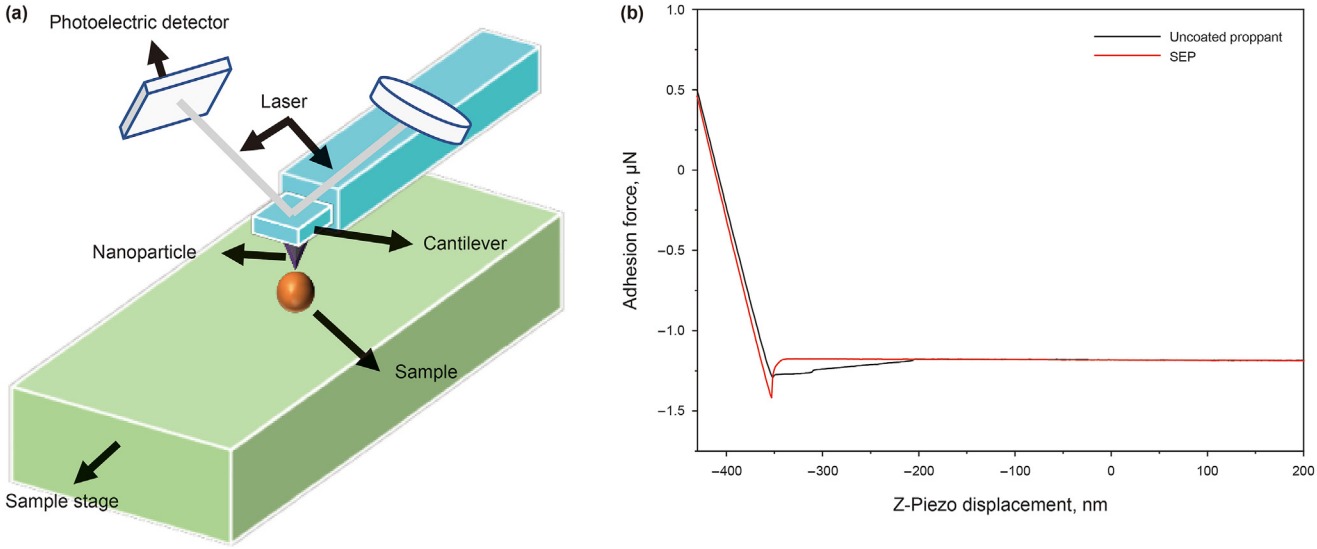

Fig. 4. (**a**) Diagrammatic sketch of the adhesion force test. (**b**) Typical AFM force curve in adhesion force measurement for a load force of 2 μN and contact time of 2.5 s.

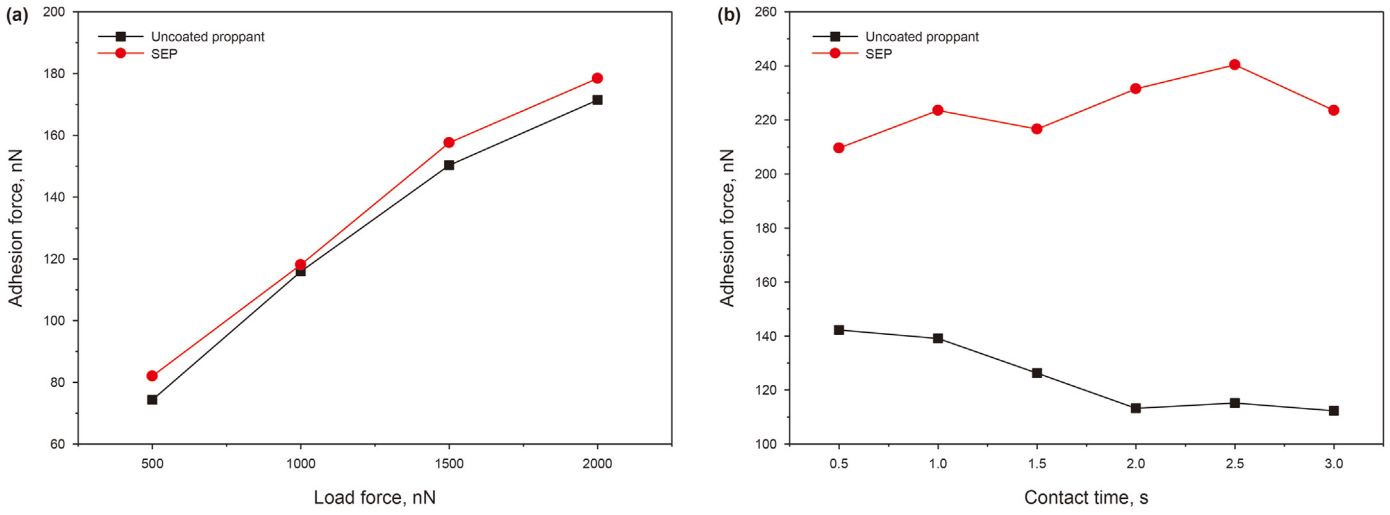

Fig. 5. Adhesion performance of the uncoated proppants and SEPs at different load forces (**a**) and contact time (**b**).

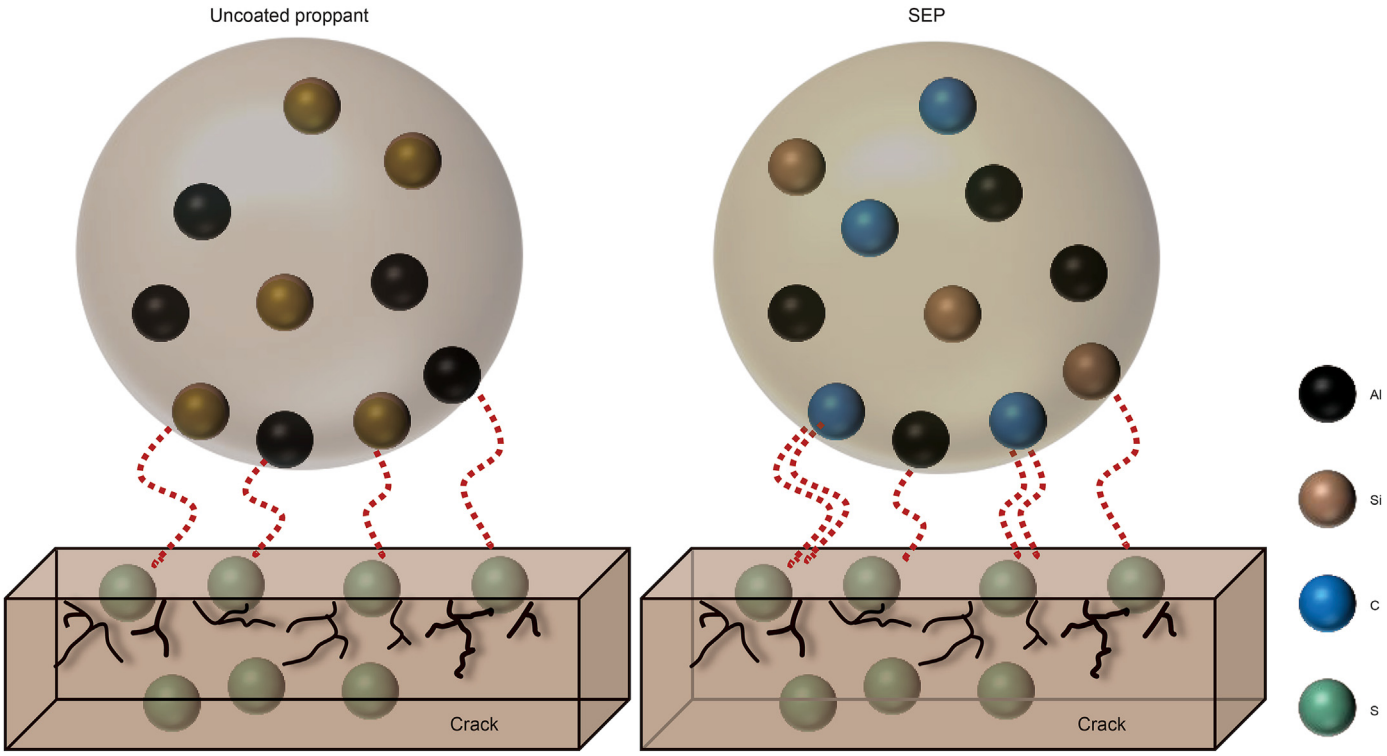

Fig. 6. Adhesion mechanism diagram of the uncoated proppants and SEPs.

of SEPs and uncoated proppant with the increased contact time. However, the adhesion force of SEPs is larger than that of uncoated proppants under the same condition, which is 47.7%, 60.7%, 71.9%, 14.06%, 104.5%, 108.7%, 99.0% higher, respectively. This demonstrates that the adhesion force of SEPs is enhanced, which prolongs the timeliness of the fracture crack. Meanwhile, proppants are easier to agglutinate together, which will improve the effect of supporting fractures.

The ceramic proppant contains aluminum and silicon, which can form covalent bonds with sulfur and silicon element of rock (Fu et al., 2016; Wu and Wu, 2012). The main force between the crack surface and proppant is the van der Waals force (Hansson et al., 2013; Ma et al. 2019, 2020). Due to the weak van der Waals force, the uncoated proppants cannot adhere to the crack surface stably. The carbon element would have free electron pairs when the proppants were coated, which can form chemical bonds with sulfur on the surface crack including cohesive bonds and hydrogen bonds (Horadam et al., 2018; Xu et al., 2014; Wu et al., 2013). In addition, as the temperature of underground rock fractures rises, the chemical bonding force between carbon and sulfur further increases with the increase (Guo et al., 2017; Tan et al., 2017; Tong and Mohanty, 2016). Because the chemical bond strength is higher than van der Waals force, the adhesion force of the SEPs is improved compared with the uncoated proppants, which will improve the fractures supporting ability (Fig. 6e) (Bandara et al., 2018; Barbati et al., 2016; Liu et al., 2016; Wang et al. 2018c, 2021).

3.2. Suspending ability

Fig. 7a shows the suspending effect of the uncoated proppants and SEPs. In the suspending experiments, the proppants were added to the guar gum solution (0.2 wt%) and constantly stirred. After standing for 15 min, 17.7 wt% of the SEPs were suspended on the surface of the guar gum solution, and 72.3 wt % of the SEPs sank to the bottom of the solution. The suspending ability (proppant weight on the surface/proppant weight at the bottom) of SEPs is 0.245. However, the weight of the uncoated proppants suspended on the surface and sank to the bottom of the guar gum solution was just 10.1% and 89.9%, respectively (Fig. 7b). The suspending ability of uncoated proppants is just 0.112. The suspending ability of SEPs is twice that of uncoated proppants. There are many pits and pores on the surface of ceramic proppants. Once the resin-epoxy is coated, the pits and pores of ceramic proppant are filled with resin-epoxy, which results in reduced proppant density. Therefore, the suspending ability of SEPs is better than the uncoated proppant. The photographs of SEPs settling experiments are shown in Fig. 7c. In settling experiments, the proppants were added to the guar gum solution of different concentrations. The settling time of the proppants in the guar gum solution was recorded. As shown in Fig. 7d, the results of settling experiments indicate that the settling time of the uncoated proppants and SEPs increased when the concentration of the guar gum solution increases. The reason is that the resistance of the solution increases with the increase in the guar gum content. Compared with the uncoated proppants, the settling time of the SEPs increased by 17.2%, 13.7%, 4%, 36.7%, 33.3%, respectively, which suggests that the SEPs migrate long distances in the fractures.

3.3. Wettability and conductivity

The contact angle experiment is conducted to evaluate the wettability of the proppants. Fig. 8a shows that the contact angle of

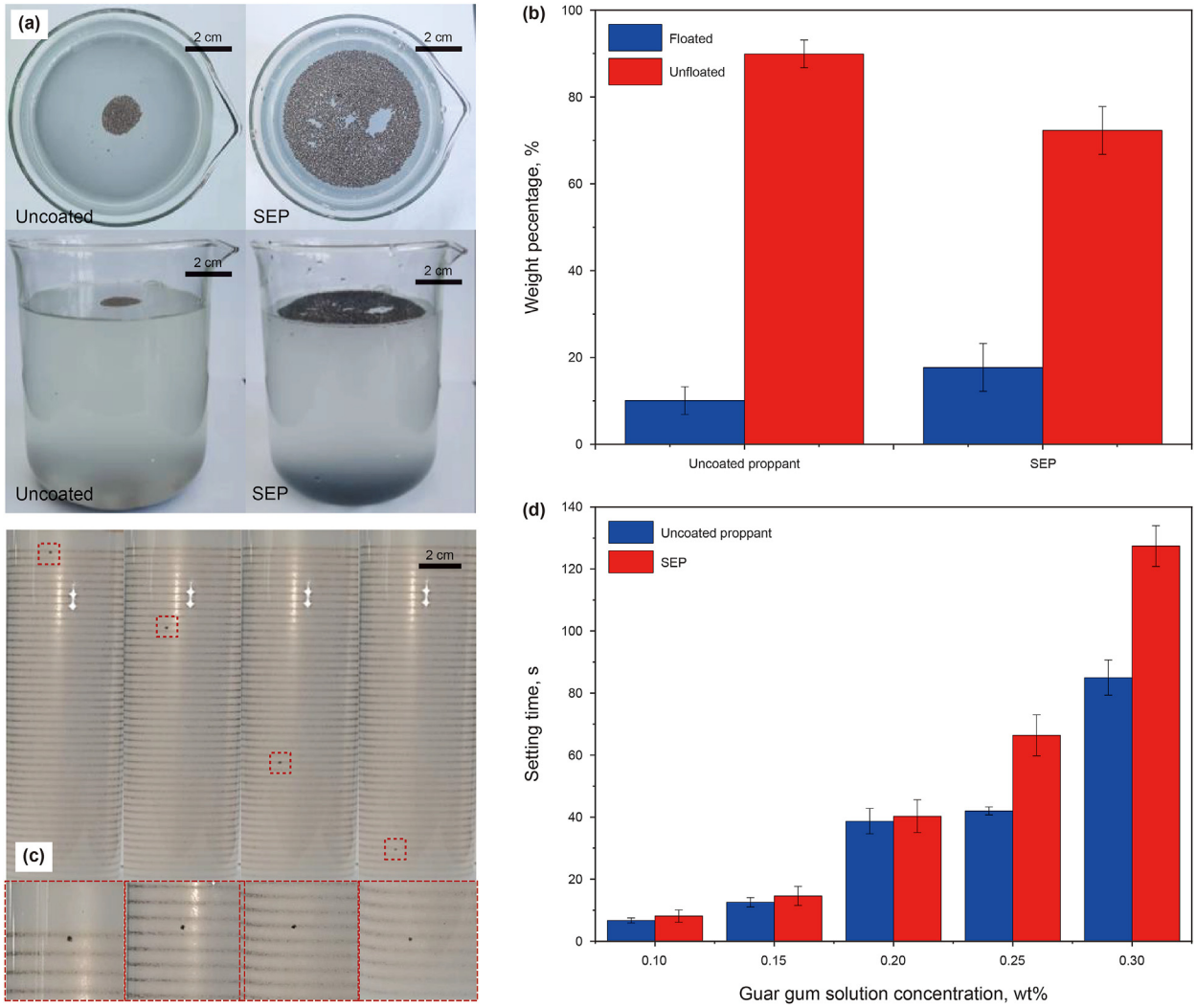

Fig. 7. (**a**) Suspending effect of the uncoated proppants and SEPs. (**b**) Results of suspending experiments of the uncoated proppants and SEPs. (**c**) Settling distance of the SEPs in the guar gum solution. (**d**) Settling time of the uncoated proppants and SEPs in the guar gum solution.

the uncoated proppants is 91.81° between water and the uncoated proppant. The contact angle is 103.66° between water and the SEPs (Fig. 8b). The contact angles of the uncoated proppants and SEPs are 94.03° and 106.60° in the guar gum solution, respectively (Fig. 8c and d). The contact angle of the SEPs increased by 13.0% and 13.4% in water and the guar gum solution, respectively, which will improve the abilities of preventing water passing through, ultimately will promote the separation of water and oil phases.

Fig. 9 shows the result of the liquid conductivity experiment of uncoated and SEPs in deionized water. The proppant concentration and the flow rate of deionized water are 5 kg/m^2 and 5 mL/min, respectively. With the increase in effective closure pressure, the liquid conductivity of uncoated proppants and SEPs reduced. The liquid conductivity of the SEPs is 17.2%, 12.5%, 7.1%, and 5.0% higher than that of the uncoated proppant, respectively. This indicates that SEPs could improve the liquid conductivity.

Fig. 10a and b shows the diagrammatic sketch of the migration and distribution of proppants in the fractures. Ceramic proppants are difficult to migrate long distances and easy to deposit at the entrance of the fracture crack, which will affect the liquid transport efficiency of proppants. The suspending and settling experiments could prove that the SEPs can migrate a longer distance in the crack, easier adhere to the fractures, which achieves better migrating and supporting effects.

The results of adhesive ability test show that the SEPs shows higher adhesion force compared with the uncoated proppant, which can improve the effect of supporting fractures. The improved suspending ability of proppant reduces the dosage and cost of proppant. The contact angle of the SEPs increased by 13.0% and 13.4% in water and the guar gum solution, respectively, which can improve the permeability of the oil phase. Moreover, the liquid conductivity of SEPs is enhanced by 17.2% at 5 MPa effective closure pressure, which can improve oil and gas transportation efficiency.

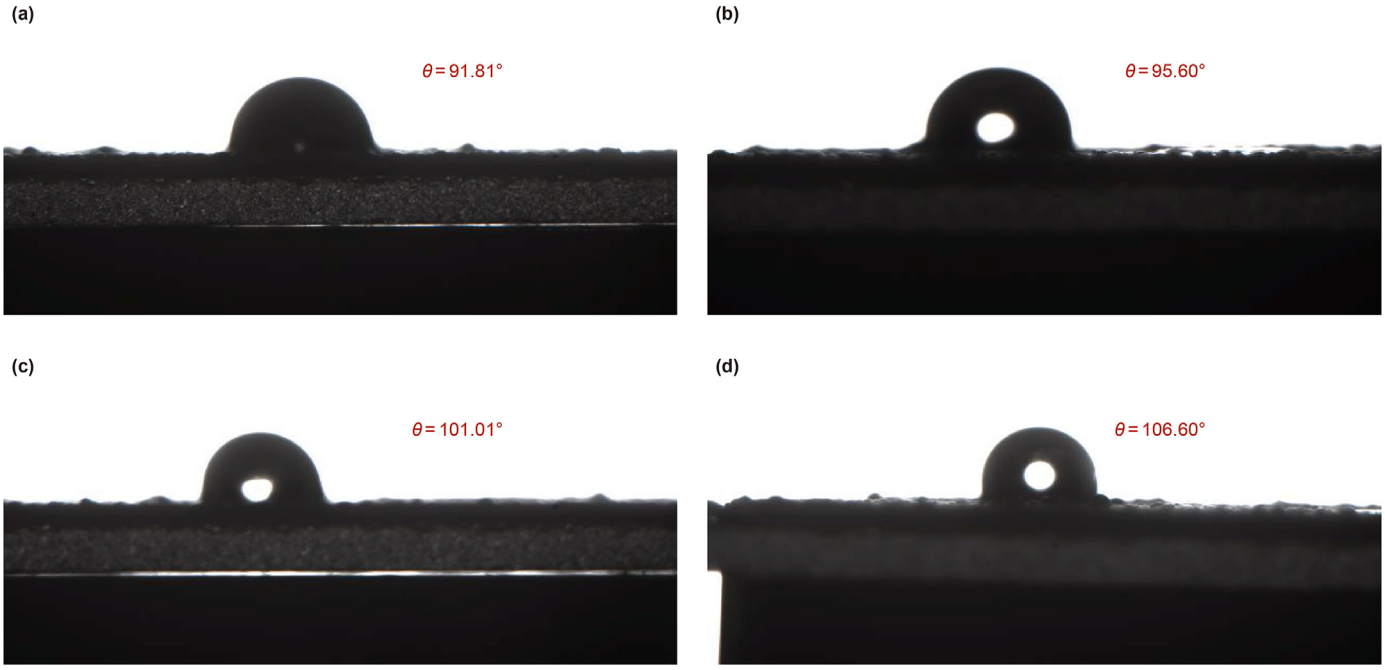

Fig. 8. Photographs of contact angles of uncoated proppants (**a**) and SEPs (**b**) in water. Photographs of contact angles of uncoated proppants (**c**) and SEPs (**d**) in the guar gum solution.

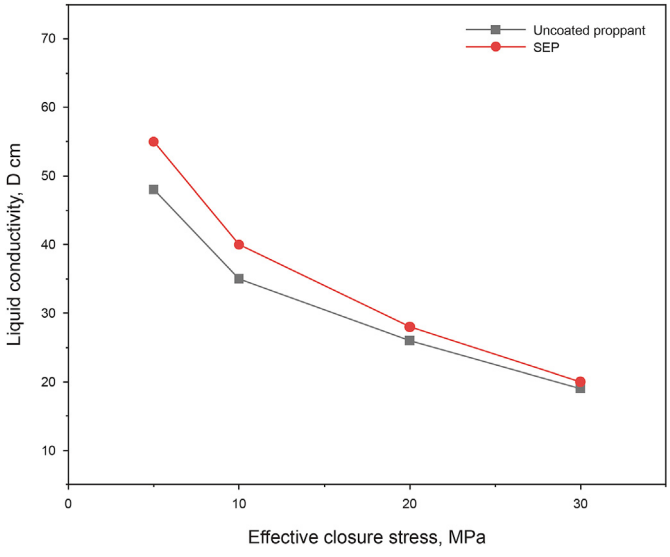

Fig. 9. Liquid conductivity of uncoated proppant and SEPs under different pressure.

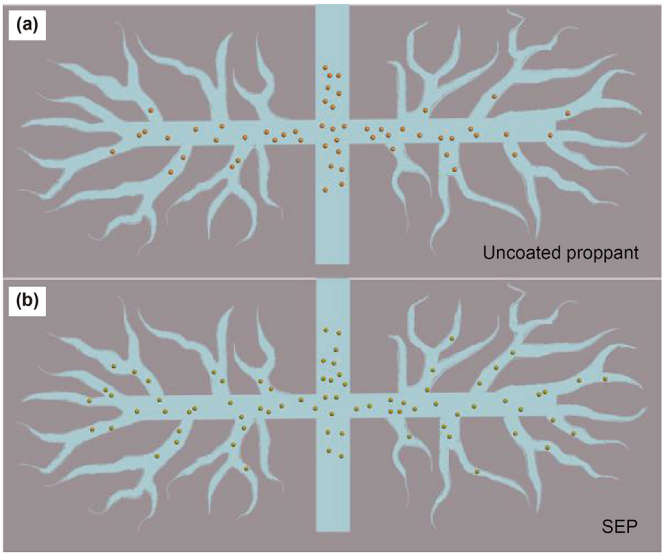

Fig. 10. Diagrammatic sketch of uncoated proppants (**a**) and SEPs (**b**).

4. Conclusions

A new double layer proppant is prepared by caoting resin-epoxy and shaly detritus on the surface of ceramic proppant, shaly detritus and epoxy-resin coated proppants (SEPs), which has improved performance compared with the traditional ceramic proppant. The suspending ability of SEPs is two times more than that of the uncoated proppants. The liquid conductivity of SEPs is 17.2% higher than the uncoated proppants at 5 MPa. Besides, the adhesive ability and wettability of SEPs are better than that of the uncoated proppants. The preparation process of SEPs provides a new shaly detritus method for shaly detritus treatment without environmental pollution.

Acknowledgments

This research was supported by the National Key Research and Development Program of China (Grant No. 2020YFC1808102), National Natural Science Foundation of China (No. 52074059), Chongqing Science Foundation for Distinguished Young Scholars (cstc2021jcyj-jqX0007) and Science Foundation of China University of Petroleum, Beijing (Nos. 2462019BJRC007, 2462019QNXZ02).

Appendix A. Supplementary data

Supplementary data to this article can be found online at https://doi.org/10.1016/j.petsci.2022.03.022.

References

Bandra, K.M.A.S., Ranjith, P.G., Rathnaweera, T.D., 2018. Proppant crushing mechanisms under reservoir conditions: insights into long-term integrity of unconventional energy production. Nat. Resour. Res. 28, 1139–1161. https://doi.org/10.1007/s11053-018-9441-0.

Bandara, K.M.A.S., Ranjith, P.G., Rathnaweera, T.D., 2020. Extensive analysis of single ceramic proppant fracture mechanism and the influence of realistic extreme reservoir conditions on proppant mechanical performance. J. Petrol. Sci. Eng. 195, 107586. https://doi.org/10.1016/j.petrol.2020.107586.

Barbati, A.C., Desroches, J., Robisson, A., McKinley, G.H., 2016. Complex fluids and hydraulic fracturing. Annu. Rev. Chem. Biomol. Eng. 7, 415–453. https://doi.org/10.1146/annurev-chembioeng-080615-033630.

Cheng, Q.Q., Li, N., Zhang, Q.L., Li, C.Y., 2020. Research progress of new coated proppants. Thermosetting Resin 35 (6), 66–70. https://doi.org/10.13650/j.cnki.rgxsz.2020.06.014 (in Chinese).

Cui, B.X., Liu, J., Chen, Y.B., Gao, F., 2017. Research progress of hydraulic fracturing proppants. Bull. Chin. Ceram. Soc. 36, 2625–2630. https://doi.org/10.16552/j.cnki.issn1001-1625.2017.08.019 (in Chinese).

Feng, Y.C., Ma, C.Y., Deng, J.G., et al., 2021. A comprehensive review of ultralow-weight proppant technology. Petrol. Sci. 18, 807–826. https://doi.org/10.1007/s12182-021-00.

Fu, L.P., Zhang, G.C., Ge, J.J., et al., 2016. Surface modified proppants used for porppant flowback control in hydraulic fracturing. Colloids Surf. A Physicochem. Eng. Asp. 507, 18–25. https://doi.org/10.1016/j.colsurfa.2016.07.039.

Guo, T.K., Li, Y.C., Ding, Y.Y., et al., 2017. Evaluation of acid fracturing treatments in shale formation. Energy Fuels 31 (10), 10479–10489. https://doi.org/10.1021/acs.energyfuels.7b01398.

Hansson, P.M., Claesson, P.M., Swerin, A., et al., 2013. Frictional forces between hydrophilic and hydrophobic particle coated nanostructured surfaces. Phys. Chem. Chem. Phys. 15 (41), 17893–17902. https://doi.org/10.1039/C3CP52196F.

Hao, J., Ma, H., Feng, X., et al., 2018. Microstructure and fracture mechanism of low density ceramic proppants. Mater. Lett. 213, 92–94. https://doi.org/10.1016/j.matlet.2017.11.021.

He, W.T., Sun, Y.H., Shan, X.L., 2021. Organic matter evolution in pyrolysis experiments of oil shale under high pressure: guidance for in situ conversion of oil shale in the Songliao Basin. J. Anal. Appl. Pyrol. 155, 105091. https://doi.org/10.1016/j.jaap.2021.105091.

Horadam, W., Venkat, N., Tran, T., et al., 2018. Leaching studies on Novolac resin-coated proppants-performance, stability, product safety, and environmental health considerations. J. Appl. Polym. Sci. 135 (8). https://doi.org/10.1002/app.45845.

Hu, X.D., Wu, K., Li, G., et al., 2018. Effect of proppant addition schedule on the proppant distribution in a straight fracture for slickwater treatment. J. Petrol. Sci. Eng. 167, 110–119. https://doi.org/10.1016/j.petrol.2018.03.081.

Kim, I., 2020. Swinging shale: shale oil, the global oil market, and the geopolitics of oil. Int. Stud. Q. 64 (3), 544–557. https://doi.org/10.1093/isq/sqaa042.

Lan, W.J., Niu, Y.C., Sheng, M., et al., 2020. Biomimicry surface-coated proppant with self-suspending and targeted adsorption ability. ACS Omega 5 (40), 25824–25831. https://doi.org/10.1021/acsomega.0c03138.

Li, W., Liu, J., Zeng, J., et al., 2020. A fully coupled multidomain and multiphysics model for evaluation of shale gas extraction. Fuel 278, 118214. https://doi.org/10.1016/j.fuel.2020.118214.

Li, G.M., Chang, X., Zhu, B.S., et al., 2018c. Sintering mechanism of high-intensity and low-density ceramic proppants prepared by recycling of waste ceramic sands. Adv. Appl. Ceram. 118, 114–120. https://doi.org/10.1080/17436753.2018.1537204.

Li, P., Zhang, X.H., Lu, X.B., et al., 2018a. Experimental study on the self-suspending proppant-laden flow in a single fracture. REM - Int. Eng. J. 71 (2), 191–196. https://doi.org/10.1590/0370-44672016.

Li, X.G., Liao, Z.J., Yang, Z.Z., et al., 2018b. Development and prospect of fracturing lightweight proppants. Bull. Chin. Ceram. Soc. 37 (10), 3132–3135. https://doi.org/10.16552/j.cnki.issn1001-1625.2018.10.019 (in Chinese).

Liu, A.P., Tian, Y.M., Zhao, P.F., et al., 2015. The development progress and future prospect of ceramic proppant. China's Ceramics 51 (6), 1–5. https://doi.org/10.16521/j.cnki.issn.1001-9642.2015.06.001 (in Chinese).

Liu, Y., Wang, D.G., Guo, Y.B., Liu, S.H., 2016. Tribological behaviors of quartz sand particles for hydraulic fracturing. Tribol. Int. 102, 485–496. https://doi.org/10.1016/j.triboint.2016.06.017.

Ma, H.Q., Tian, Y.M., Li, G.M., 2019. Effects of sintering temperature on microstructure, properties, and crushing behavior of ceramic proppants. Int. J. Appl. Ceram. Technol. 16 (4), 1450–1459. https://doi.org/10.1111/ijac.13204.

Ma, H.Q., Bao, C.G., Tian, T.M., Li, G.M., 2020. Effects of feldspar content on microstructure and property for high-strength corundum-mullite proppants. Trans. Indian Ceram. Soc. 79 (1), 18–22. https://doi.org/10.1080/0371750X.2019.1699863.

Man, S., Wong, R.C., 2017. Compression and crushing behavior of ceramic proppants and sand under high stresses. J. Petrol. Sci. Eng. 158, 268–283. https://doi.org/10.1016/j.petrol.2017.08.052.

Mocciaro, A., Lombardi, M.B., Scian, A.N., 2018. Effect of raw material milling on ceramic proppants properties. Appl. Clay Sci. 153, 90–94. https://doi.org/10.1016/j.clay.2017.12.009.

Neto, L.B., Khanna, A., Kotousov, A., 2015. Conductivity and performance of hydraulic fractures partially filled with compressible proppant packs. Int. J. Rock. Mech. Min. 74, 1–9. https://doi.org/10.1016/j.ijrmms.2014.11.005.

Osiptsov, A.A., 2017. Fluid mechanics of hydraulic fracturing: a review. J. Petrol. Sci. Eng. 156, 513–535. https://doi.org/10.1016/j.petrol.2017.05.019.

Reinicke, A., Rybacki, E., Stanchits, S., et al., 2010. Hydraulic fracturing stimulation techniques and formation damage mechanisms—implications from laboratory testing of tight sandstone–proppant systems. Geochemistry 70, 107–117. https://doi.org/10.1016/j.chemer.2010.05.016.

Ren, Y., Ren, Q., Wu, X., et al., 2019. Mechanism of low temperature sintered high-strength ferric-rich ceramics using bauxite tailings. Mater. Chem. Phys. 238, 121929. https://doi.org/10.1016/j.matchemphys.2019.121929.

Tan, Y.L., Pan, Z.J., Liu, J.L., et al., 2017. Experimental study of permeability and its anisotropy for shale fracture supported with proppant. J. Nat. Gas Sci. Eng. 44, 250–264. https://doi.org/10.1016/j.jngse.2017.04.020.

Tang, Y., Ranjith, P.G., Perera, M.S.A., 2018. Major factors influencing proppant behaviour and proppant-associated damage mechanisms during hydraulic fracturing. Acta Geotechnica 13 (4), 757–780. https://doi.org/10.1007/s11440-018-0670-5.

Thomas, L., Tang, H.S., Kalyon, D.M., et al., 2019. Toward better hydraulic fracturing fluids and their application in energy production: a review of sustainable technologies and reduction of potential environmental impacts. J. Petrol. Sci. Eng. 173, 793–803. https://doi.org/10.1016/j.petrol.2018.09.056.

Tong, S.Y., Mohanty, K.K., 2016. Proppant transport study in fractures with intersections. Fuel 181, 463–477. https://doi.org/10.1016/j.fuel.04.144.

Wang, H., Sharma, M.M., 2018. Modeling of hydraulic fracture closure on proppants with proppant settling. J. Petrol. Sci. Eng. 171, 636–645. https://doi.org/10.1016/j.petrol.2018.07.067.

Wang, J.H., Elsworth, D., 2018. Role of proppant distribution on the evolution of hydraulic fracture conductivity. J. Petrol. Sci. Eng. 166, 249–262. https://doi.org/10.1016/j.petrol.2018.03.040.

Wang, M., Guo, Z.Q., Jiao, C.X., 2019. Exploration progress and geochemical features of lacustrine shale oils in China. J. Petrol. Sci. Eng. 178, 975–986. https://doi.org/10.1016/j.petrol.2019.04.029.

Wang, T.Y., Tian, S.C., Li, G.S., et al., 2021. Molecular simulation of gas adsorption in shale nanopores: a critical review. Renew. Sustain. Energy Rev. 149, 111391. https://doi.org/10.1016/j.rser.2021.111391.

Wang, T.Y., Tian, S.C., Li, G.S., et al., 2018. Molecular simulation of CO_2/CH_4 competitive adsorption on shale kerogen for CO_2 sequestration and enhanced gas recovery. J. Phys. Chem. C 122 (30), 17009–17018. https://doi.org/10.1021/acs.jpcc.8b02061.

Wei, G., Babadagli, T., Huang, H., et al., 2020. A visual experimental study: resin-coated ceramic proppants transport within rough vertical models. J. Petrol. Sci. Eng. 191, 107142. https://doi.org/10.1016/j.petrol.2020.107142.

Wu, T.T., Wu, B.L., Zhao, M., 2013. Acid resistance of silicon-free ceramic proppant. Mater. Lett. 92, 210–212. https://doi.org/10.1016/j.matlet.2012.10.124.

Wu, T.T., Wu, B.L., 2012. Corrosion resistance of ceramic proppant in $BaO–CaO–P_2O_5–Al_2O_3$ system. Corrosion Sci. 63, 399–403. https://doi.org/10.1016/j.corsci.2012.06.025.

Wu, X.L., Huo, Z.Z., Ren, Q., et al., 2017. Preparation and characterization of ceramic proppants with low density and high strength using fly ash. J. Alloys Compd. 702, 442–448. https://doi.org/10.1016/j.jallcom.2017.01.262.

Xie, X.K., Niu, S.X., Miao, Y., et al., 2019. Preparation and properties of resin coated ceramic proppants with ultra light weight and high strength from coal-series kaolin. Appl. Clay Sci. 183, 105364. https://doi.org/10.1016/j.clay.2019.105364.

Xu, Q., Li, M., Zhang, L.P., et al., 2014. Dynamic adhesion forces between microparticles and substrates in water. Langmuir 30 (37), 11103–11109. https://doi.org/10.1021/la502735w.

Xu, Q., Fan, F., Lu, Z., et al., 2021. Reversible adhesion surface coating proppant. Chin. Chem. Lett. 32 (1), 553–556. https://doi.org/10.1016/j.cclet.2020.02.014.

Xu, Y.B., Sun, P.C., Yao, S.Q., 2019. Progress in exploration, development and utilization of oil shale in China. Oil Shale 36 (2), 285–304. https://doi.org/10.3176/OIL.2019.2.03.

Yao, C., Shao, J.F., Jiang, Q.H., et al., 2019. A new discrete method for modeling hydraulic fracturing in cohesive porous materials. J. Petrol. Sci. Eng. 180, 257–267. https://doi.org/10.1016/j.petrol.2019.05.051.

Zhang, G.D., Gutierrez, M., Li, M.Z., 2017a. Numerical simulation of transport and placement of multi-sized proppants in a hydraulic fracture in vertical wells. Granul. Matter 19 (2), 32. https://doi.org/10.1007/s10035-017-0718-5.

Zhang, J.C., 2014. Theoretical conductivity analysis of surface modification agent treated proppant. Fuel 134, 166–170. https://doi.org/10.1016/j.fuel.2014.05.031.
Zhang, J.J., Ouyang, L.C., Zhu, D., Hill, A.D., 2015. Experimental and numerical studies of reduced fracture conductivity due to proppant embedment in the shale reservoir. J. Petrol. Sci. Eng. 130, 37–45. https://doi.org/10.2118/170775-MS.
Zhang, X.F., Yunan, S.C., Han, X.R., et al., 2017b. Experimental and theoretical study of fracture conductivity with heterogeneous proppant placement. J. Nat. Gas Sci. Eng. 37, 449–461. https://doi.org/10.1016/j.jngse.2016.11.059.